Icosahedron $[Cl_{12}]^{12-}$ Templated Gigantic $Gd_{158}Co_{38}$ Nanocluster with the Largest Ln_{158} Core for Magnetic Cooling

Li Liningfang
Nanjing Tech University
Ximing Luo
Nanjing Tech University
Jia Wang
Nanjing University
Jilei Wang
Nanjing Tech University
You Song
Nanjing University, Nanjing 210023 https://orcid.org/0000-0002-0289-7830
Hua Mei
Nanjing Tech University
Yan Xu (yanxu@njtech.edu.cn)
Nanjing Tech University https://orcid.org/0000-0001-6059-075X

Article

Keywords: synthesis, physical chemistry, clusters

Posted Date: July 26th, 2021

DOI: https://doi.org/10.21203/rs.3.rs-699859/v1

Abstract

The synthesis of large nano-sized cluster-molecules is a goal that synthesists and structural scientists have been pursuing, as well as a huge challenge. Herein, the largest 3d-4f metal clusters **Cl_{12}@$Gd_{158}Co_{38}$** and **Br_{12}@$Gd_{158}Co_{38}$** until now are obtained through the "multi-anions-template" strategy, with a protein-sized metal frame (*ca.* 4.3 × 3.6 × 3.5 nm^3). Different from the mixed distribution of 3d and 4f metals and the hollow structure in the previous giant 3d-4f clusters, for the dense core-shell structure **Cl_{12}@$Gd_{158}Co_{38}$** and **Br_{12}@$Gd_{158}Co_{38}$**, the Ln_{158} core with the highest Ln nuclearity number is induced by icosahedra-shaped templates $[Cl_{12}]^{12-}$ or $[Br_{12}]^{12-}$, while 3d metals (Co) are distributed on its periphery. Their appearances point out a new structure type of non-open giant Ln-based clusters (metal number > 100) and provide an ideal model for studying the multi-level assembly of complex macromolecules. Additionally, **Cl_{12}@$Gd_{158}Co_{38}$** shows the largest magnetic entropy change ($-\Delta S_m^{max}$ = 46.95 J kg^{-1} K^{-1} under 2.0 K and ΔH = 7 T) among reported high-nuclearity 3d-4f clusters.

Introduction

Synthesis and structural characterization of giant molecules have long been one of the most attractive fields, owing to their fascinating topological structures, complex intramolecular assembly behavior, and numerous physical-chemical properties different from small molecules[1–10]. High-nuclearity lanthanide(Ln)-containing clusters are one of the new members of the giant molecular family and has received extensive attention in the past decade associated with charming structures and excellent properties in magnetism, catalysis, and luminescence[11–20].

Ongoing progress in synthetic strategy (such as anion template, mixed-ligand, building blocks strategy, *etc.*[21–26]) has enabled the preparation of giant Ln(4f)-exclusive clusters (such as $\{Ln_{104}\}$[27], $\{Ln_{140}\}$[28]) and transition-lanthanide(3d-4f) clusters (such as $\{La_{68}Ni_{90}\}$[24], $\{La_{76}Ni_{88}\}$[24], $\{Gd_{78}Ni_{64}\}$,[29] $\{Ln_{96}Ni_{64}\}$[23], and $\{Gd_{102}Ni_{36}\}$[30]). However, successful preparation and vigorous development of other giant metal clusters (for instance, $\{Ag_{490}\}$[31], $\{Mo_{368}\}$[32], $\{Nd_{288}\}$[33], $\{Mo_{248}\}$[34], and $\{La_{10}Ni_{48}Sb_{16}W_{140}\}$[35] with 214 metal ions) illustrated that the exploration of giant 4f-containing clusters is almost the tip of the iceberg, mainly due to various and complicated coordination modes of lanthanide ions, huge uncertainty in synthesis[36].

Compared to 4f-exclusive clusters, it proves that 3d-4f clusters seem to have better synthetic controllability and may have both the advantages of different metals and potential synergistic effects. On the basis of the mentioned above synthetic methods, Kong, Zheng, and Xu *et al.* fabricated a series of high-nuclearity 3d-4f clusters[21–26]. Unfortunately, 3d-4f compounds with more than 100 metal ions were only realized in the Ni-Ln system and featured the similar metal arrangement and open hollow structure types, which were frequently based on the multi-dentate ligand iminodiacetic acid (H_2IDA)[24,37]. Recently, Zheng's group constructed a wheel $\{Gd_{102}Ni_{36}\}$ high-nuclearity cluster without H_2IDA ligand, through utilizing SO_4^{2-}-templates and Ni-complexes as protected groups located at the outer vertices of the

cluster[30]. The emergence of this cluster suggests that giant Ni-Ln nano-clusters can also perform the wheel structure, which seems to echo the wheel-shaped $\{Gd_{140}\}$[28]. Attempting at assembly 3d and 4f ions into giant clusters featured novel and charming configurations differing from the above two kinds of forms, is promising and challenging.

Relative to the extensive research on the synthesis and properties of Ni-Ln, other high-nuclearity 3d-Ln clusters are less studied, owing to the difficulty of synthesis[38–39]. Co ions with the high spin ground state and excellent catalysis have been widely studied[40–44]. For instance, $\{Ln_{42}Co_{10}\}$, and $\{Ln_{45}Co_7\}$ possess the outstanding magnetocaloric effect than similar structures of $\{Ln_{42}Ni_{10}\}$ and $\{Ln_{45}Ni_7\}$[5,45]. In 2021, a series of $\{Ln_{36}Co_{12}\}$[46] clusters were obtained on the basis of $\{Ln_{36}Ni_{12}\}$[22] and presented the higher electrocatalytic activity. Meanwhile, $\{Ln_{42}Co_{10}\}$[5], and $\{Ln_{45}Co_7\}$[45], both with 52 metal ions, are so far largest Co-Ln clusters, indicating that the development of Co-Ln materials is far inferior to Ni-Ln. These facts encourage us to explore and synthesize giant Co-Ln clusters, expecting to obtain various structures and diversified excellent properties from the existing ones.

In this work, a fantastic high-nuclearity heterometallic cluster with a 4.3 nm size, $[Cl_{12}@Gd_{158}Co_{38}(CO_3)_{90}(OAc)_{18}(\mu_3\text{-}OH)_{236}(CH_3NH_2CH_2COO)_6(MIDA)_{42}(H_2O)_{84}]\cdot Cl_{24}\cdot 144(H_2O)$ and $[Br_{12}@Gd_{158}Co_{38}(CO_3)_{90}(OAc)_{18}(\mu_3\text{-}OH)_{236}(CH_3NH_2CH_2COO)_6(MIDA)_{42}(H_2O)_{78}(CH_3O)_6]\cdot Cl_{12}\cdot Br_6\cdot 94(H_2O)$ (abbreviated as **$Cl_{12}@Gd_{158}Co_{38}$**, **$Br_{12}@Gd_{158}Co_{38}$**, H_2MIDA = N- methyliminodiacetic acid, HOAc = acetic acid), were obtained via icosahedron-like $[Cl_{12}]^{12-}$ or $[Br_{12}]^{12-}$ anionic templates. According to the metal nuclearity number, alluring **$Cl_{12}@Gd_{158}Co_{38}$** and **$Br_{12}@Gd_{158}Co_{38}$** clusters both contain the largest number of metal ions (196) in previous 3d-4f compounds, and are more than *ca.* 4 times of reported largest Co-4f metal clusters[5,45]. Another amusing feature of two compounds is the presence of new highest-nuclearity Ln-OH aggregate $[Gd_{158}(CO_3)_{66}(\mu_3\text{-}OH)_{236}]$ (**Gd_{158}**). The existence of multiple isotropic anionic templates (12 Cl^- or Br^-) plays a vital role in the formation and stability of the inner **Gd_{158}**. What is more, the inner **Gd_{158}** is protected by multi-ligands and 38 Co ions to form the captivating **$Cl_{12}@Gd_{158}Co_{38}$** and **$Br_{12}@Gd_{158}Co_{38}$** clusters. To the best of our knowledge, the emergence of **$Cl_{12}@Gd_{158}Co_{38}$** and **$Br_{12}@Gd_{158}Co_{38}$** nanoclusters make the structural configurations of 3d-4f cluster family more abundant, which breaks the traditional cavity structure[21–26]. Simultaneously, numerous Gd^{3+} ions make **$Cl_{12}@Gd_{158}Co_{38}$** and **$Br_{12}@Gd_{158}Co_{38}$** clusters display the potential magnetic cooling application with much larger value of $-\Delta S_m^{max}$ (46.30 and 46.95 and J kg^{-1} K^{-1} under 2.0 K and ΔH = 7 T) among the identified 3d-4f metal clusters.

Results

Structure analysis. Single-crystal X-ray diffraction (SCXRD) demonstrates that the structure of **$Cl_{12}@Gd_{158}Co_{38}$** is similatr to **$Br_{12}@Gd_{158}Co_{38}$**, here only **$Cl_{12}@Gd_{158}Co_{38}$** as example to be discussed in

detail. **Cl_{12}@$Gd_{158}Co_{38}$** crystallizes in the trigonal crystal system, *R*-3 space group. The cationic core of **Cl_{12}@$Gd_{158}Co_{38}$** constitutes of six Cl_{12}@$Gd_{27}Co_7(CO_3)_{15}(OAc)_4(\mu_3\text{-}OH)_{40}(CH_3NH_2CH_2COO)(MIDA)_7(H_2O)_{14}$ (**Cl_{12}@$Gd_{27}Co_7$**, in which Gd4, Co4, and O29 are distributed in the C_3 axis) building units (Fig. 1a, 1b). **Cl_{12}@$Gd_{27}Co_7$** is made up of one highly symmetrical cationic unit $Gd_{26}Co_5(CO_3)_{15}(OAc)_3(\mu_3\text{-}OH)_{40}(MIDA)_7(H_2O)_{14}$ (**$Gd_{26}Co_5$**) and two Cl^- anionic templates, one Gd, two Co ions, one OAc^-, and one $CH_3NH_2CH_2COO^-$ ligand (decomposition of H_2MIDA, Fig. S14, Scheme S2). In addition, **$Gd_{26}Co_5$** (Fig. 1c) can be regarded as three different motifs: type I, formulated as $Gd_5Co_2(MIDA)_2(OAc)(CO_3)_3(\mu_3\text{-}OH)_4$ (**Gd_5Co_2**), is distributed in the top of **$Gd_{26}Co_5$**; type II, formulated as $Gd_{16}(MIDA)_2(CO_3)_9(\mu_3\text{-}OH)_{22}$ (**Gd_{16}**), is distributed in the middle of **$Gd_{26}Co_5$**; type III, formulated as $Gd_5Co_3(MIDA)_3(OAc)(CO_3)_2(\mu_3\text{-}OH)_4$ (**Gd_5Co_3**), is distributed in the bottom of **$Gd_{26}Co_5$**. Besides, two $Gd_7(MIDA)(CO_3)_3(\mu_3\text{-}OH)_{11}$ (**Gd_7**, Fig. 1e) is connected by two $Gd(CO_3)$ to form **Gd_{16}**. Based on four CO_3^{2-} and four μ_3-OH^- groups, **Gd_5Co_2**, **Gd_{16}**, and **Gd_5Co_3** motifs are joined together to form **$Gd_{26}Co_5$**. **Cl_{12}@$Gd_{158}Co_{38}$** has a 3-fold symmetric (C_3) axis and an inversion center (Fig. S11-12). Three asymmetric building units **Cl_{12}@$Gd_{27}Co_7$** obtained by rotation are connected together alternately via CO_3^{2-} and μ_3-OH^- anions to form a trimer $Gd_{79}Co_{19}(CO_3)_{45}(OAc)_{12}(\mu_3\text{-}OH)_{120}(CH_3NH_2CH_2COO)_3(MIDA)_{21}$ (**$Gd_{79}Co_{19}$**). Two trimers **$Gd_{79}Co_{19}$** obtained by inversion are further joined into **$Gd_{158}Co_{38}$**.

It is worth noting that a large series of CO_3^{2-} anions as important templates and linkers among metal ions, deriving from the decomposition of organic ligands, exhibit a rich variety of coordination modes (Fig. S3), reflecting the complexity of the nanocluster structure, and the adaptability of the anion templates. Meanwhile, the main ligand $MIDA^{2-}$ also shows unusual and diverse coordination modes (Fig. S4). For example, high chemical affinity of N atom from organic ligands tends to coordinate with 3d ions[38], but N atoms in this work are also linked with 4f ions.

Interestingly, in **Cl_2@$Gd_{27}Co_7$**, two crystallographically independent halide ions (Cl1 and Cl2) are found in the center of similar two Gd-CO_3-OH cages [$(Gd_{16}(CO_3)_6(\mu_3\text{-}OH)_7$, Fig. 2a, 2c], hydrogen-bonded to 7 μ_3-OH^- groups, respectively (Fig. 2d, 2f, distance of Cl···O: from 3.219 Å to 3.419 Å, angle of Cl-H-O: from 155.15° to 176.16°)[22]. Additionally, six Cl1 and six Cl2 ions obtained by rotainversion form one icosahedron $[Cl_{12}]^{12-}$ cage (**Cl_{12}**, distance of Cl···Cl: from 7.216 Å to 8.445 Å, Fig. 2e, 3b). The 12 Gd-CO_3-OH cages templated by Cl^- ions form the main structure $[Gd_{116}(CO_3)_{66}(\mu_3\text{-}OH)_{84}]$ (Fig. 2b) of Ln-core $[Gd_{158}(CO_3)_{66}(\mu_3\text{-}OH)_{236}]$ by sharing 4f metals or anions (CO_3^{2-} and OH^-). Although Cl^- ions as the templates in metal clusters have been obtained (such as $\{Gd_{36}Ni_{12}\}$[22] templated by 2 Cl^-; $\{Gd_8Cr_4\}$[47] templated by one Cl^- and one ClO_4^-), this 3d-4f nanocluster with more than ten Cl^- templates (**Cl_{12}** with one icosahedron pattern) is firstly reported, and it has important guiding significance for the prediction and construction of high-nuclearity 4f-containing nanoclusters.

For the sake to facilitate the illustration and comprehending of the complex metal skeleton, **Cl_{12}@$Gd_{158}Co_{38}$** can be disassembled into three components (Fig. S15): (i) six $Gd(MIDA)_2(CO_3)(\mu_3\text{-}OH)_2$ groups, exhibiting a near-octahedral geometry; (ii) six $Co(MIDA)_3$ groups, showing a hexagonal arrangement; (iii) one $Cl_{12}@Gd_{152}Co_{32}(CO_3)_{24}(\mu_3\text{-}OH)_{116}$ group (**Cl_{12}@$Gd_{152}Co_{32}$**), revealing a typical core-shell structure and modular features. From the inside to outside, **Cl_{12}@$Gd_{152}Co_{32}$** (Fig. 3 and S16) is treated as **Gd_{20}@Cl_{12}@$Gd_{48}Co_{32}$@$(Gd)_{12}$@$(Gd_{12})_6$**, and presents one dodecahedron Ln-core of 20 Gd^{3+} ions $[Gd_{20}(CO_3)_{12}]$ (**Gd_{20}**, Fig. 3a), one icosahedron of 12 Cl^- ions (**Cl_{12}**, Fig. 3b), one truncated-cube-like cage of **$Gd_{132}Co_{32}$** (Fig. 3i). **$Gd_{132}Co_{32}$** comprised of eight propeller-like heterometallic building blocks $[Gd_6Co_4(\mu_3\text{-}OH)_9]$ (**Gd_6Co_4**, Fig. 3e) as truncated-cubic vertices forming main metal framework $[Gd_{48}Co_{32}(\mu_3\text{-}OH)_{44}]$ (**$Gd_{48}Co_{32}$**, Fig. 3d), 12 $Gd(\mu_3\text{-}OH)_3$ groups (**Gd**, Fig. 3f) as edges, six saddle-shaped motifs ($[Gd_{12}(CO_3)_2(\mu_3\text{-}OH)_6]$, **$Gd_{12}$**, Fig. 3g) as faces. So, **$Gd_{132}Co_{32}$** can be viewed as $(Gd_6Co_4)_8@(Gd)_{12}@(Gd_{12})_6$. Here are 10 Co^{3+} and 28 Co^{2+} ions in final products, determined by XPS (Fig. S33) and charge balance.

Althrough the metal structures of **Br_{12}@$Gd_{158}Co_{38}$** and **Cl_{12}@$Gd_{158}Co_{38}$** are very similar, ther are some difference between two compound: (i) six CH_3O ligands and 30 anions (12 Cl^- and 18 Br^-) are exisisted in **Br_{12}@$Gd_{158}Co_{38}$** to balace the charge balance; (ii) but 36 anions (30 Cl^-) are exisisted in **Cl_{12}@$Gd_{158}Co_{38}$**.

Magnetic properties. The large presence of metal ions inspires us to investigate the magnetic properties of **Br_{12}@$Gd_{158}Co_{38}$** and **Cl_{12}@$Gd_{158}Co_{38}$**. The plot of temperature-dependent magnetic susceptibility ($\chi_M T$-T) was studied under 1.0 kOe direct current (dc) field with the scope of 1.8–300 K (Fig. S38, S39). The $\chi_M T$ values under the room temperature were 1380.75 (**Cl_{12}@$Gd_{158}Co_{38}$**) and 1384.91 (**Br_{12}@$Gd_{158}Co_{38}$**) $cm^3\ K\ mol^{-1}$, which is bigger than the theoretical value of 1296.75 $cm^3\ K\ mol^{-1}$ for 158 uncorrelated Gd^{3+} ($S = 7/2$, $g = 2$) and 28 high-spin Co^{2+} ($S = 3/2$, $g = 2$)[45]. The difference between the theoretical and test values is put down to the remarkable orbital contributions of the high-spin Co^{2+} ions[5]. As the temperature goes down, the value of $\chi_M T$ gradually decreases and achieves 726.25 (**Cl_{12}@$Gd_{158}Co_{38}$**) and 696.30 (**Br_{12}@$Gd_{158}Co_{38}$**) $cm^3\ K\ mol^{-1}$ at 1.8 K. This behavior is mainly ascribed to the depopulation of Kramers excited state levels of octahedral coordination environment for Co^{2+} ion because the magnetic interaction between 3d and 4f or 4f and 4f ions. Based on the Curie-Weiss Law, fitting the plot of χ_M^{-1} versus T shows parameters, [$C = 1415\ cm^3\ K\ mol^{-1}$ and $\theta = -6.04$ K (**Cl_{12}@$Gd_{158}Co_{38}$**); $C = 1462.60\ cm^3\ K\ mol^{-1}$ and $\theta = -3.20$ K (**Br_{12}@$Gd_{158}Co_{38}$**)], for the sum contribution of orbital of Co^{2+} ion and the coupling between metal ions (Fig. S40, S41). The field-dependent magnetization (M-H) of **Cl_{12}@$Gd_{158}Co_{38}$** was performed in the range of 1.8–20 K at 0–7 T (Fig. S42, S43). The curves of M vs H represent a steady rise in magnetization and attain 1045.29 $N\mu_B$ (**Cl_{12}@$Gd_{158}Co_{38}$**) and 1058.57 $N\mu_B$ (**Br_{12}@$Gd_{158}Co_{38}$**) $N\mu_B$ at 7 T at 1.8 K, which are slightly lesser than the expected value 1190 $N\mu_B$ for 158 uncorrelated Gd^{3+} ($S = 7/2$, $g = 2$) and 28 high-spin Co^{2+} ($S = 3/2$, $g = 2$)[45]. It also results from the orbital effect of Co^{2+}, which gives an effective spin $S_{eff} = 1/2$ and the

magnetization is usually ~ 2.1 $N\mu_B$ per Co^{2+} ion[48].A large class of Gd^{3+} ions in $\mathbf{Cl_{12}@Gd_{158}Co_{38}}$ and $\mathbf{Br_{12}@Gd_{158}Co_{38}}$ urge us to explore its magnetocaloric effect. The calculated magnetic entropy changes ΔS_m were evaluated via using the Maxwell relation ($\Delta S_m(T) = \int [\partial M(T, H)/\partial T]_H \, dH$)[29]. As shown in Fig. 4, S44, the values of $-\Delta S_m^{max}$ are 46.95 ($\mathbf{Cl_{12}@Gd_{158}Co_{38}}$) and 46.30 ($\mathbf{Br_{12}@Gd_{158}Co_{38}}$) J kg^{-1} K^{-1} at 2.0 K at 7 T. The values are smaller than their theoretical values (64.33 and 62.32 J kg^{-1} K^{-1}) by applying the formula of $-\Delta S_m = nR\ln(2S+1)$, which are attributable to the presence of possible antiferromagnetic interaction[30]. Nevertheless, their values were much larger than known 3d-4f cluster complexes (Table S6). And the value of $\mathbf{Cl_{12}@Gd_{158}Co_{38}}$ is the largest at present. In low magnetic field, $\mathbf{Br_{12}@Gd_{158}Co_{38}}$ and $\mathbf{Cl_{12}@Gd_{158}Co_{38}}$ also show prominent magnetocaloric effect with $-\Delta S_m$ = 20.13, 20.81 J kg^{-1} K^{-1} at 2.0 K and 2 T, respectively (Table S7)[49].

Discussion

In summarize, two charming and giant 3d-4f nanoclusters (*ca.* 4.3 × 3.6 × 3.5 nm^3) have been successfully synthesized using "$[Cl_{12}]^{12-}$ or $[Br_{12}]^{12-}$ templates" in the presence of multidentate organic ligand (H_2MIDA). 4f metal core ($\mathbf{Gd_{158}}$) is protected by 38 Co ions and small ligands to form $\mathbf{Br_{12}@Gd_{158}Co_{38}}$ and $\mathbf{Cl_{12}@Gd_{158}Co_{38}}$, which both contain 196 metal ions to be the largest 3d-4f cluster until now. In addition, abundant Gd^{3+} ions make $\mathbf{Cl_{12}@Gd_{158}Co_{38}}$ and $\mathbf{Br_{12}@Gd_{158}Co_{38}}$ show potential magnetic cooling materials with $-\Delta S_m^{max}$ = 46.95 and 46.30 J kg^{-1} K^{-1}, at 2 K for ΔH = 7 T, which are much larger than known 3d-4f clusters. This work not only overcomes the traditional cavity structure, but also provides one entertaining assumption of high-nuclearity 3d-4f metal frameworks. Next, we will try our best to prepare more 3d-4f molecular magnetocaloric materials through anion-template method.

Methods

Material and Instrumentation. All materials were of merchant origin and were used firsthand. The Perkin-Elmer 2400 elemental analyzer was used to perform Elemental analyses (EA; C, H and N). Under room temperature enviromrnt, powder X-ray diffraction (PXRD) was documented (collected in the range of 3 – 50°.) on a Bruker D8X diffractometer furnished with monochromatized Cu-K_α under λ = 1.5418 Å radiation. Infrared spectra (IR) was recorded (from 4000 to 400 cm^{-1}) by pressed KBr pellets with a Nicolet Impact 410 FTIR spectrometer. TGA (thermogravimetric analysis and differential scanning calorimeter measurement) was recorded among 25 to 900°C in a flowing nitrogen environment with a heating degree of 10 K·min^{-1} via the NETZSCH STA409 thermogravimetric analyzer. The ZSX Primus II was used to analuze the X-ray fluorescence (XRF) spectrometry. The Hitachi S-4800 scanning electron microscope was carried out to analyze the SEM images and energy dispersive spectrometer (EDS), with a stimulative voltage of 20 kV. The direct current magnetic data (temperature of 1.8–300 K), and the magnetisation isothermal measurements (field with 0–7 T) were obtained on MPMS-XL7 SQUID magnetometer. Experimental susceptibilities were revisional for the diamagnetism estimated Pascal's

tables and for products holder by antecedently calibration. The KRATOS AXIS SUPRA™ spectrometer, outfitted with a monochromatized Al Kα source, wsa used to record X-ray photoelectron spectroscopy (XPS). The charge effect was trued via using the binding energy of C1s (284.8 eV) to weaken the sample charging influence.

Synthesis of $Cl_{12}@Gd_{158}Co_{38}$. The mixture of $GdCl_3 \cdot 6H_2O$ (0.185 g, 0.5 mmol), $Co(OAc)_2 \cdot 6H_2O$ (0.120 g, 0.5 mmol), N-Methyliminodiacetic acid (H_2MIDA; 0.077 g, 0.5 mmol), imidazole (0.068 g, 1 mmol) were melted in deionized water (4 mL), ethanol (5 mL), methanol (1 mL), which was stirred with 2 hours under about 25 ℃. Finally, the mixture was heated 72 h with 160°C. Octahedron-like pink crystals were collected by filtration and washed by deionized water (61.33 % based on Gd). Elemental analyses for $C_{354}H_{1124}Gd_{158}Co_{38}N_{48}O_{950}Cl_{36}$, calculated (%): C, 8.56; H, 2.26; N, 1.35; found (%): C, 8.62 H, 2.23; N, 1.28.

Synthesis of $Br_{12}@Gd_{158}Co_{38}$. The mixture of $Gd(NO_3)_3 \cdot 6H_2O$ (0.223 g, 0.5 mmol), $Co(OAc)_2 \cdot 6H_2O$ (0.120 g, 0.5 mmol), KBr (0.119 g, 1mmol), N-Methyliminodiacetic acid (H_2MIDA; 0.077 g, 0.5 mmol), imidazole (0.068 g, 1 mmol) were melted in deionized water (4 mL), ethanol (5 mL), methanol (1 mL), which was stirred with 2 hours under about 25 ℃ and the pH was adjusted to 4.5 with HCl (1 M). Finally, the mixture was heated 72 h with 160°C. Octahedron-like pink crystals were collected by filtration and washed by deionized water (61.33 % based on Gd). Elemental analyses for $C_{360}H_{1030}Br_{18}Cl_{12}Co_{38}Gd_{158}N_{48}O_{900}$, calculated (%): C, 8.75; H, 2.09; N, 1.36; found (%): C, 8.69; H, 2.12; N, 1.45.

Declarations

Data availability. Data supporting the findings of this manuscript are available from the corresponding authors upon reasonable request. The X-ray crystallographic coordinates for structures reported in this article have been deposited at the Cambridge Crystallographic Data Centre (CCDC) under deposition number CCDC: 2090809 ($\mathbf{Cl_{12}@Gd_{158}Co_{38}}$), 2090810 ($\mathbf{Br_{12}@Gd_{158}Co_{38}}$).

Acknowledgments

This work was supported by the National Key R&D Program of China (2018YFA0306004), the Natural Science Foundation of China (21571103 and 21973038), Jiangsu Province (BK20191359), the Joint Fund for Regional Innovation and De-velopment (U20A2073).

Author contributions

Y.X. conceived and designed the experiments. N.F.L., J.W., J.L.W., conducted the synthesis and characterization. X.M.L., N.F.L. drew pictures in the manuscript. X.M.L., N.F.L., Y.S., Y.X., H.M., analyzed the experimental results. X.M.L., N.F.L., Y. S., Y. Xu co-wrote the manuscript.

Additional information

Supplementary information is available in the online version of the paper. Reprints and permissions information is available online at www.nature.com/reprints. Correspondence and requests for materials should be addressed to Y. Xu.

Competing financial interests

The authors declare no competing financial interests.

References

1. Zheng, Y.-Z., Zheng, Z. &. Chen, X.-M. A symbol approach for classification of molecule-based magnetic materials exemplified by coordination polymers of metal carboxylates, *Coord. Chem. Rev.* **258**, 1-15 (2014).
2. Zheng, X.-Y., Xie, J., Kong, X.-J., Long, L.-S. & Zheng, L.-S. Recent advances in the assembly of high-nuclearity lanthanide clusters. *Coord. Chem. Rev.* **378**, 222-236 (2019).
3. Zheng, Y.-Z., Evangelisti, M. & Winpenny, R. E. P. Co–Gd phosphonate complexes as magnetic refrigerants. *Chem. Sci.* **2**, 99-102 (2011).
4. Chen, W. P. et al. Quantum Monte Carlo simulations of a giant $\{Ni_{21}Gd_{20}\}$ cage with a $S = 91$ spin ground state. *Nat. Commun.* **9**, 1-6 (2018).
5. Gui, L. C., Wang, X. J., Ni, Q. L., Wang, M., Liang, F. P. & Zou, H. H. Nanospheric $[M_{20}(OH)_{12}(maleate)_{12}(Me_2NH)_{12}]^{4+}$ clusters (M = Co, Ni) with O_h symmetry. *J. Am. Chem. Soc.* **134**, 852-854 (2012).
6. Zheng, Y. Z., Zhou, G. J., Zheng, Z. & Winpenny, R. E. P. Molecule-based magnetic coolers. *Chem. Soc. Rev.* **43**, 1462-1475 (2014).
7. Geng, D. et al. Merohedral icosahedral M_{48} ($M = Co^{II}, Ni^{II}$) cage clusters supported by thiacalix[4]arene. *Chem. Sci.* **9**, 8535-8541 (2018).
8. Liu, J. H. et al. All-inorganic open frameworks based on gigantic four-shell $Ln@W_8@Ln_8@(SiW_{12})_6$ clusters. *Chem. Commun.* **56**, 10305-10308 (2020).
9. Wang, J., Liu, X., Du, Z. & Xu, Y. Organo-functionalized polyoxovanadates: crystal architecture and property aspects. *Dalton Trans.* **50**, 7871-7886 (2021).
10. Li, X.-Y. et al. A Giant Dy_{76} Cluster: A New Fused Bi-Nanopillar Structural Model in Lanthanide Clusters. *Angew. Chem., Int. Ed.* **131**, 10290-10294 (2019).
11. Chen, L. et al. A novel 2-D coordination polymer constructed from high-nuclearity waist drum-like pure Ho_{48} clusters. *Chem. Commun.* **49**, 9728-9730 (2013).
12. Cui, C., Cao, J. P., Luo, X. M., Lin, Q. F. & Xu, Y. Two Pairs of Chiral "Tower-Like" Ln_4Cr_4 (Ln=Gd, Dy) Clusters: Syntheses, Structure, and Magnetocaloric Effect. *Chem. Eur. J* **24**, 15295-15302 (2018).
13. Dong, J., Cui, P., Shi, P. F., Cheng, P. & Zhao, B. Ultrastrong Alkali-Resisting Lanthanide-Zeolites Assembled by $[Ln_{60}]$ Nanocages. *J. Am. Chem. Soc.* **137**, 15988-15991 (2015).

14. Chen, R., Yan, Z. H., Kong, X. J., Long, L. S. & Zheng, L. S. Integration of Lanthanide-Transition-Metal Clusters onto CdS Surfaces for Photocatalytic Hydrogen Evolution. *Angew. Chem., Int. Ed.* **57**, 16796-16800 (2018).
15. Rinck, J. et al. An octanuclear $[Cr^{III}_4Dy^{III}_4]$ 3d-4f single-molecule magnet. *Angew. Chem., Int. Ed.* **49**, 7583-7587 (2010).
16. Luo, X. M. et al. Exploring the Performance Improvement of Magnetocaloric Effect Based Gd-Exclusive Cluster Gd_{60}. *J. Am. Chem. Soc.* **140**, 11219-11222 (2018).
17. Galico, D. A., Kitos, A. A., Ovens, J. S., Sigoli, F. A. & Murugesu, M. Lanthanide-Based Molecular Cluster-Aggregates: Optical Barcoding and White-Light Emission with Nanosized $\{Ln_{20}\}$ Compounds. *Angew. Chem., Int. Ed.* **60**, 6130-6136 (2021).
18. Zheng, X. Y. et al. Insights into Magnetic Interactions in a Monodisperse $Gd_{12}Fe_{14}$ Metal Cluster. *Angew. Chem., Int. Ed.* **56**, 11475-11479 (2017).
19. Qin, L. et al. Topological Self-Assembly of Highly-Symmetric Lanthanide Clusters: A Magnetic Study of Exchange-Coupling "Fingerprints" in Giant Gadolinium(III) Cages. *J. Am. Chem. Soc*. **139**, 16405-16411 (2017).
20. Qin, L. et al. A "Molecular Water Pipe": A Giant Tubular Cluster $\{Dy_{72}\}$ Exhibits Fast Proton Transport and Slow Magnetic Relaxation. *Adv. Mater.* **28**, 10772-10779 (2016).
21. Li, N. F., Lin, Q. F., Luo, X. M., Cao, J. P. & Xu, Y. Cl^--Templated Assembly of Novel Peanut-like $Ln_{40}Ni_{44}$ Heterometallic Clusters Exhibiting a Large Magnetocaloric Effect. *Inorg. Chem.* **58**, 10883-10889 (2019).
22. Peng, J. B. A 48-metal cluster exhibiting a large magnetocaloric effect. *Angew. Chem., Int. Ed.* **50**, 10649-10652 (2011).
23. Chen, W. P., Liao, P. Q., Yu, Y., Zheng, Z., Chen, X. M. & Zheng, Y. Z. A Mixed-Ligand Approach for a Gigantic and Hollow Heterometallic Cage $\{Ni_{64}RE_{96}\}$ for Gas Separation and Magnetic Cooling Applications. *Angew. Chem., Int. Ed.* **55**, 9375-9379 (2016).
24. Du, M.-H., Zheng, X.-Y., Kong, X.-J., Long, L.-S. & Zheng, L.-S. Synthetic Protocol for Assembling Giant Heterometallic Hydroxide Clusters from Building Blocks: Rational Design and Efficient Synthesis. *Matter* **3**, 1334-1349 (2020).
25. Luo, X.-M., Li, N.-F., Lin, Q.-F., Cao, J.-P., Yuan, P. & Xu, Y. A single-ligand-protected $Eu_{60-n}Gd(Tb)_n$ cluster: a reasonable new approach to expand lanthanide aggregations. *Inorg. Chem. Front.* **7**, 2072-2079 (2020).
26. Kong, X. J., Long, L. S., Huang, R. B., Zheng, L. S., Harris, T. D. & Zheng, Z. A four-shell, 136-metal 3d-4f heterometallic cluster approximating a rectangular parallelepiped. *Chem. Commun.* **29**, 4354-4356 (2009).
27. Peng, J. B. et al. Beauty, symmetry, and magnetocaloric effect-four-shell keplerates with 104 lanthanide atoms. *J. Am. Chem. Soc.* **136**, 17938-17941 (2014).

28. Zheng, X. Y. et al. A Gigantic Molecular Wheel of $\{Gd_{140}\}$: A New Member of the Molecular Wheel Family. *J. Am. Chem. Soc.* **139**, 18178-18181 (2017).
29. Lin, Q. F., Li, J., Luo, X. M., Cui, C. H., Song, Y. & Xu, Y. Incorporation of Silicon-Oxygen Tetrahedron into Novel High-Nuclearity Nanosized 3d-4f Heterometallic Clusters. *Inorg. Chem.* **57**, 4799-4802 (2018).
30. Chen, W. P. et al. The Gigantic $\{Ni_{36}Gd_{102}\}$ Hexagon: A Sulfate-Templated "Star-of-David" for Photocatalytic CO_2 Reduction and Magnetic Cooling. *J. Am. Chem. Soc.* **142**, 4663-4670 (2020).
31. Anson, C. E. et al. Synthesis and crystal structures of the ligand-stabilized silver chalcogenide clusters $[Ag_{154}Se_{77}(dppxy)_{18}]$, $[Ag_{320}(S\mathit{t}Bu)_{60}S_{130}(dppp)_{12}]$, $[Ag_{352}S_{128}(S\mathit{t}C_5H_{11})_{96}]$, and $[Ag_{490}S_{188}(S\mathit{t}C_5H_{11})_{114}]$. *Angew. Chem., Int. Ed.* **47**, 1326-1331 (2008).
32. Müller, A., Beckmann, E., Bögge, H., Schmidtmann, M. & Dress, A. Inorganic chemistry goes protein size: a Mo_{368} nano-hedgehog initiating nanochemistry by symmetry breaking. *Angew. Chem. Int. Ed.* **41**, 1162-1167 (2002).
33. Wu, Y. L., Li, X. X., Qi, Y. J., Yu, H., Jin, L. & Zheng, S. T. $\{Nb_{288}O_{768}(OH)_{48}(CO_3)_{12}\}$: A Macromolecular Polyoxometalate with Close to 300 Niobium Atoms. *Angew. Chem., Int. Ed.* **57**, 8572-8576 (2018).
34. Müller, A., Shah, S. Q. N., Bögge, H. & Schmidtmann, M. Molecular growth from a Mo_{176} to a Mo_{248} cluster. *Nature* **397**, 48-50 (1999).
35. Li, S. R. et al. A Giant 3d-4f Polyoxometalate Super-Tetrahedron with High Proton Conductivity. *Small Methods* **5**, 2000777-2000783 (2020).
36. Peng, J. B. et al. High-nuclearity 3d-4f clusters as enhanced magnetic coolers and molecular magnets. *J. Am. Chem. Soc.* **134**, 3314-3317 (2012).
37. Kong, X. J. et al. A four-shell, nesting doll-like 3d-4f cluster containing 108 metal ions. *Angew. Chem., Int. Ed.* **47**, 2398-2401 (2008).
38. Zhang, H.-G., Du, Y.-C., Yang, H., Zhuang, M.-Y., Li, D.-C. & Dou, J.-M. A new family of $\{Co_4Ln_8\}$ metallacrowns with a butterfly-shaped structure. *Inorg. Chem. Front.* **6**, 1904-1908 (2019).
39. Yu, Y. et al. A Series Three-Dimensional Ln_4Cr_4 (Ln = Gd, Tb, Er) Heterometallic Cluster-Based Coordination Polymers Containing Interesting Nanotubes Exhibiting High Magnetic Entropy. *Inorg. Chem.* **59**, 5593-5599 (2020).
40. Zhang, Z. M. et al. Wheel-shaped nanoscale 3d-4f $\{Co^{II}_{16}Ln^{III}_{24}\}$ clusters (Ln = Dy and Gd). *Chem. Commun.* **49**, 8081-8083 (2013).
41. Zheng, S. T., Wu, T., Irfanoglu, B., Zuo, F., Feng, P. & Bu, X. Multicomponent self-assembly of a nested $Co_{24}@Co_{48}$ metal-organic polyhedral framework. *Angew. Chem., Int. Ed.* **50**, 8034-8037 (2011).
42. Han, H., Ding, Y.-S., Zhu, X., Han, T., Zheng, Y.-Z. & Liao, W. Constructing $[Co^{II}_6]$ hexagon-centered heterometallic $\{Ln_6Co_6\}$ (Ln = Y, Eu and Dy) clusters with a calix[8]arene ligand. *Inorg. Chem. Front.* **7**, 4070-4076 (2020).

43. Lun, H. J., Du, M. H., Wang, D. H., Kong, X. J., Long, L. S. & Zheng, L. S. Double-Propeller-like Heterometallic 3d-4f Clusters $Ln_{18}Co_7$. *Inorg. Chem.* **59**, 7900-7904 (2020).
44. Zheng, Y. Z., Evangelisti, M., Tuna, F. & Winpenny, R. E. P. Co-Ln mixed-metal phosphonate grids and cages as molecular magnetic refrigerants. *J. Am. Chem. Soc.* **134**, 1057-1065 (2012).
45. Fan, S. et al. Four 3d–4f heterometallic $Ln_{45}M_7$ clusters protected by mixed ligands. *CrystEngComm* **20**, 2120-2125 (2018).
46. Chen, R. et al. Soluble lanthanide-transition-metal clusters $Ln_{36}Co_{12}$ as effective molecular electrocatalysts for water oxidation. *Chem. Commun.* **57**, 3611-3614 (2021).
47. Yin, J.-J., Chen, C., Zhuang, G.-L., Zheng, J., Zheng, X.-Y. & Kong, X.-J. Anion-Dependent Assembly of 3d-4f Heterometallic Clusters Ln_5Cr_2 and Ln_8Cr_4. *Inorg. Chem.* **59**, 1959-1966 (2020).
48. Mishra, V., Lloret, F. & Mukherjee, R. Coordination versatility of 1,3-bis[3-(2-pyridyl)pyrazol-1-yl]propane: Co(II) and Ni(II) complexes. *Inorg. Chim. Acta.* **359**, 4053-4062 (2006).
49. Li, N., Lin, Q., Han, Y., Du, Z. & Xu, Y. The chain-shaped coordination polymers based on the bowl-like $Ln_{18}Ni_{24(23.5)}$ clusters exhibiting favorable low-field magnetocaloric effect. *Chin. Chem. Letter.* **2021**, DOI: 10.1016/j.cclet.2021.04.042.

Figures

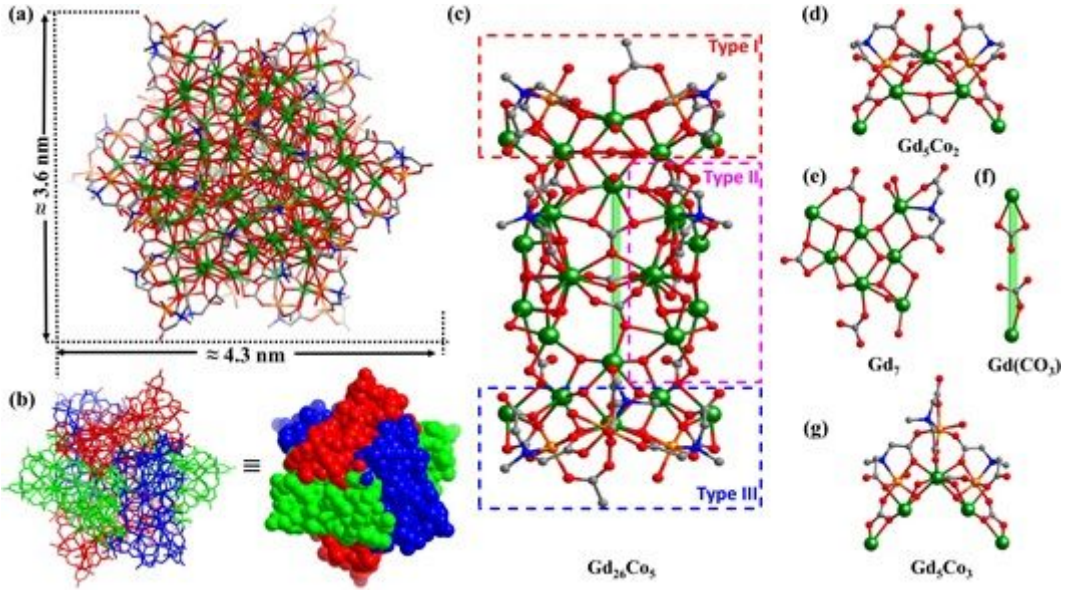

Figure 1

Single-crystal X-ray structure of Cl12@Gd158Co38. a Ball-and-stick graph of Cl12@Gd158Co38. b The assembly diagram of Cl12@Gd158Co38 based on Cl2@Gd27Co7 building units. c Ball-and-stick view of Gd26Co5. d Ball-and-stick view of Gd5Co2. e Ball-and-stick view of Gd7. f Ball-and-stick view of Gd(CO3). g Ball-and-stick view of Gd5Co3. Color codes: green, Gd; orange, Co; blue: N; red, O; gray, C.

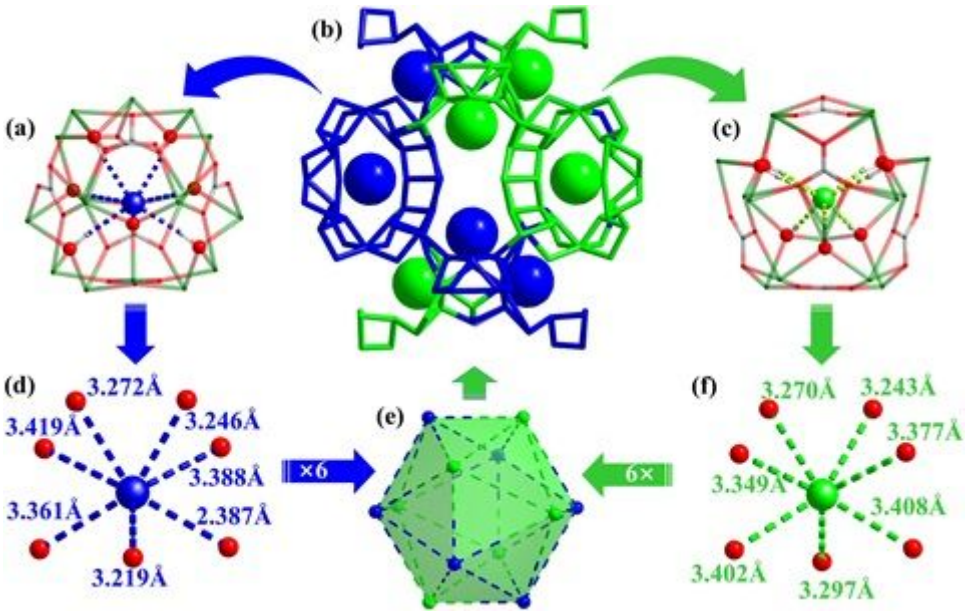

Figure 2

Metal assembly based on [Cl12]12- template. a Ball-and-stick graph of Gd16(CO3)6(μ3-OH)7 templated by crystallographically independent Cl1. b Simplified representation of [Gd116(CO3)66(μ3-OH)84] templated by Cl12. c Ball-and-stick view of Gd16(CO3)6(μ3-OH)7 templated by crystallographically independent Cl2 (c); d The magnified hydrogen-bonding interactions from Cl1. e Icosahedron Cl12. f The magnified hydrogen-bonding interactions from Cl2. Color codes: green, Gd; red, O; gray, C; blue: Cl1; bright green: Cl2.

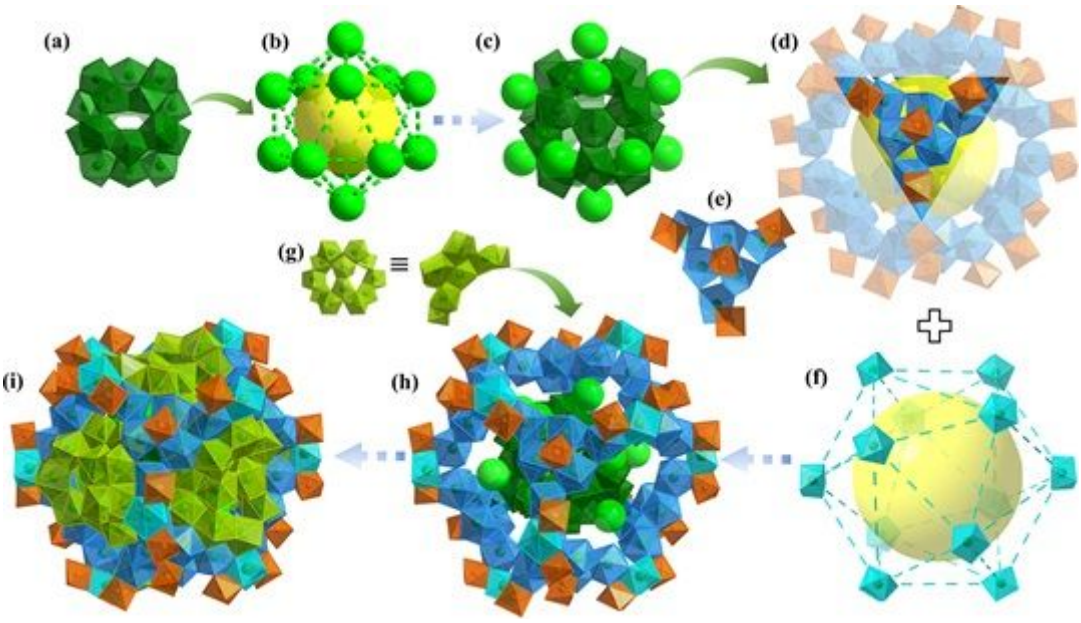

Figure 3

Building blocks Cl12@Gd158Co38. a Polyhedron graph of Gd20 dodecahedron. b Ball-and-stick graph of Cl12 icosahedron. c The perspective graph of Gd20@Cl12. d the near-cubic metal framework of Gd48Co32. e The propeller-like motif Gd6Co4. f The polyhedron view of 12 Gd with an icosahedron

pattern. g The saddle-shaped motif Gd12. h Polyhedron view of Gd20@Cl12@Gd48Co32@(Gd)12. i Polyhedron view of Gd20@Cl12@Gd48Co32@(Gd)12@(Gd12)6. Polyhedral color codes: green (Gd20), pale blue (Gd from Gd48Co32), turquoise (Gd), lime (Gd12), orange, Co. Atomic color codes: green, Gd; orange, Co; bright green, Cl.

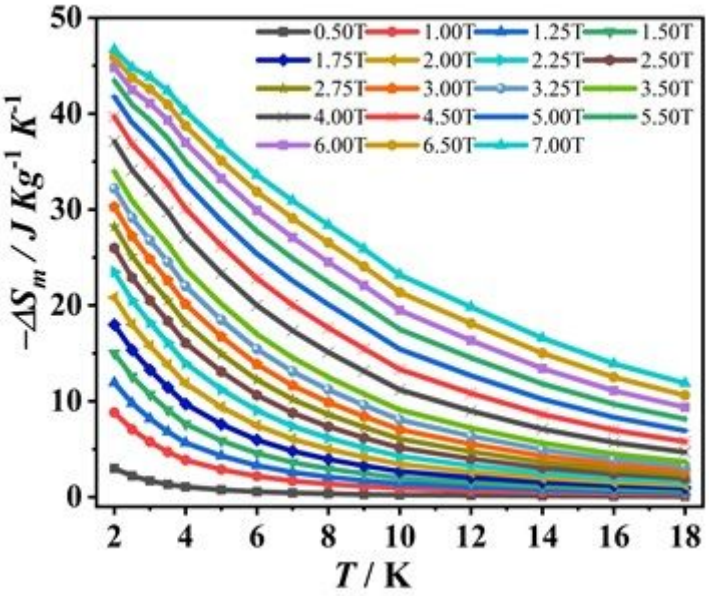

Figure 4

The magnetic characteristics of Cl12@Gd158Co38. Values of -ΔSm calculated from the magnetization data for Cl12@Gd158Co38 at various fields (0.50-7.00 T) and temperatures (1.8 - 18 K).

Supplementary Files

This is a list of supplementary files associated with this preprint. Click to download.

- SupportingInformation.docx